University of Birjand

Water Harvesting Research (2026) Vol. 9, No. 1: 140-154

10.22077/jwhr.2026.11799.1209

ORIGINAL ARTICLE

Multiannual Soil-Erosion Potential and Structural Connectivity in the Deli Watershed, Southwestern Iran (2005–2025)

Kohzad Heidary[a*], Amin Zoratipour[b]

[a]Department of Soil Conservation and Watershed Management Research, Khuzestan Agricultural and Natural Resource Research Center, Agricultural Research, Education and Extension Organization, Ahvaz, Iran.
[b]Department of Natural Engineering, Faculty of Agriculture, Khuzestan University of Agricultural Sciences and Natural Resources, Ahvaz, Iran.

[*]Corresponding Author E-mail Address: k.heidary@areeo.ac.ir

Received: 30 July 2026, **Revised**: 04 September 2026, **Accepted**: 20 September 2026

Abstract

Water erosion in semi-arid mountain watersheds depends on both sediment-source potential and the structural connection of source areas to the drainage network. A multiannual, sensitivity-aware screening workflow was developed for the 105.20 km² Deli watershed, southwestern Iran, for 2005–2025. Landsat 5/7 indices were transformed to an Operational Land Imager-equivalent scale using local near-coincident Landsat 7–8 pairs, annual cover-management factors were derived, rainfall erosivity was represented using a CHIRPS–modified Fournier proxy, soil erodibility was estimated from SoilGrids, and topographic controls were derived from a 30 m DEM. Annual RUSLE products were combined with structural connectivity, hotspot persistence and conditional support-practice scenarios. The uncertainty measure is the low-to-high structural sensitivity range across alternative R, K, C and P assumptions, not a probabilistic confidence interval. All erosion and delivery results are unitless comparative index values rather than physical soil-loss or sediment-yield rates. The long-term mean potential soil-loss index was 582.11 index units; annual means ranged from 138.33 in 2010 to 1040.20 in 2018, with no significant monotonic watershed-scale trend. The annual response closely followed the rainfall-erosivity proxy (Spearman $\rho = 0.98$, $p < 0.001$), whereas its association with the watershed-mean C factor was weak and non-significant ($\rho = -0.07$, $p = 0.758$). Hotspots recurring in at least half of the years occupied 10.42 km², and mean relative structural uncertainty was 37.40%. Moderate and strong conditional P scenarios, representing 10–45% and 55–72.5% local reductions across eligible cells, lowered the index within 4.85 km² of stable cropland by 36.87% and 68.38%, but reduced the watershed-wide mean by only 0.34% and 0.63% because the treated domain covered about 4.6% of the watershed. The maps provide first-tier evidence for prioritizing field verification, monitoring and sediment pre-treatment. CHIRPS intensity limitations, the approximately 250 m support of SoilGrids and the absence of sediment observations preclude calibrated rates or stand-alone siting decisions.

Keywords: Conservation screening, Deli watershed, Multiannual rusle, Rainfall-erosivity proxy, Structural sediment connectivity

1. Introduction

Soil erosion by water is both an on-site land-degradation process and an off-site water-management problem. Detachment and redistribution reduce effective soil depth, organic matter and nutrient stocks, while sediment delivered to channels increases turbidity, degrades aquatic habitats and shortens the service life of reservoirs and water-harvesting structures (Renard et al. 1997; Borrelli et al. 2021). These effects are especially consequential in semi-arid mountain watersheds, where erosive storms are intermittent, vegetation cover is spatially discontinuous and runoff can become rapidly concentrated along structurally controlled drainage lines (Borrelli et al. 2020; Heckmann et al. 2018). Global assessments indicate that changes in land use and rainfall regimes may alter erosion risk substantially, but they also show that prediction remains sensitive to model structure, data scale and management assumptions (Borrelli et al. 2020 & 2021). Consequently, a useful watershed assessment must distinguish evidence supported by observations from model-derived hypotheses requiring field confirmation.

The Revised Universal Soil Loss Equation (RUSLE) remains one of the most widely used empirical frameworks because its factors can be represented spatially and its data requirements are modest relative to physically based models. Its widespread use, however, has encouraged interpretations beyond its original domain. RUSLE estimates long-term sheet and rill erosion potential; without local calibration it should not be reported as measured soil loss, and it does not explicitly simulate gully erosion, bank erosion, within-channel transport or deposition (Renard et al. 1997; Benavidez et al. 2018). Recent reviews have therefore recommended that RUSLE outputs be treated as comparative indicators when independent sediment records are unavailable (Borrelli et al. 2021). This distinction is particularly important in water-harvesting planning, where the relevance of a source depends not only on its potential production but also on whether sediment can reach a channel, reservoir or harvesting structure.

Sediment-connectivity analysis addresses this missing source-to-sink dimension. Structural indices evaluate how contributing area, slope, pathway length and surface resistance combine to facilitate or impede transfer from a hillslope cell to a specified target (Borselli et al. 2008; Cavalli et al. 2013). Such indices identify potential sediment-source areas and structurally connected pathways; they do not establish functional or event-scale sediment transfer without flux observations. Here, structural connectivity denotes landscape propensity for transfer, whereas functional connectivity denotes realized transfer during a specific event and is not estimated in this study (Heckmann et al. 2018; Najafi et al. 2021; Shi et al. 2025). Their value is therefore greatest when coupled with explicit uncertainty statements, sensitivity analysis and field verification. Recent integrated approaches further show that connectivity and hotspot information can make conservation screening more selective than erosion-intensity maps alone (Batista et al. 2022; La Licata et al. 2025).

A second limitation of conventional watershed assessments is temporal compression. Using one land-cover map and one long-term rainfall average suppresses years of extreme forcing and treats recovery or degradation of surface cover as stationary. Cloud computing and the long Landsat archive now permit annual reconstruction of vegetation and moisture conditions (Gorelick et al. 2017; Barbadori et al. 2024). Nevertheless, a 21-year record spanning Landsat Thematic Mapper, Enhanced Thematic Mapper Plus and Operational Land Imager sensors cannot be interpreted reliably without cross-sensor harmonization, because spectral-response differences can mimic land-surface change (Roy et al. 2016). Similar scale cautions apply to rainfall and soils: Climate Hazards Group InfraRed Precipitation with Station data (CHIRPS) and Soil Grids provide consistent regional information, but resampling them to a 30 m computational grid does not create 30 m climatic or pedological information (Funk et al. 2015; Poggio et al. 2021).

The Deli watershed was selected as a demanding test case because its erosion problem cannot be reduced to a single remotely sensed variable. Historical field surveys combined field reconnaissance, soil-profile description, laboratory analysis, aerial-photograph interpretation and geomorphological mapping.

They documented folded-Zagros terrain, erodible marl and siltstone units, locally bare hillslopes, rill and gully development, stream-bank erosion and downstream sediment transfer towards the Jarreh Reservoir system (Deli Watershed Detailed Studies Project 2008a & 2008b). These 2008 observations provide historical process context only; they neither verify present land management nor constitute co-registered validation of the 2005–2025 model products.

Previous research in Khuzestan has shown that cell-scale structural connectivity can distinguish likely sediment-transfer pathways (Zoratipour and Heidary 2022). However, Iranian evidence integrating multiannual RUSLE forcing with connectivity remains limited, and no previous Deli assessment resolved the combined effects of sensor discontinuity, temporal hotspot persistence, source-to-stream connection, scenario scale and input sensitivity.

Comparable semi-arid mountain assessments commonly use a single land-cover snapshot or long-term rainfall mean, resample regional products without retaining their native-scale limitations, or analyses erosion intensity and connectivity separately (Benavidez et al. 2018; Zoratipour and Heidary 2022; La Licata et al. 2025). The present workflow fills this gap by integrating locally harmonized annual forcing, persistent upper-decile source areas, structural pathway information and sensitivity-qualified scenarios, while explicitly restricting the outputs to spatial screening.

Accordingly, the aims were (i) to estimate annual rainfall-erosivity and harmonized cover-management factors for 2005–2025; (ii) calculate annual RUSLE-based potential soil-loss indices without assigning unsupported mass units; (iii) identify spatially persistent potential hotspots and their structural connection to a reference drainage network; (iv) quantify sensitivity to alternative rainfall, soil, cover and support-practice assumptions; and (v) compare baseline, moderate and strong conditional management scenarios. Our working hypothesis was that climatic erosivity would govern the amplitude of year-to-year variation, whereas relief, surface resistance and structural connectivity would govern where critical source areas persisted. Rather than seeking one definitive erosion number, the study was designed to identify where field verification and protection of water-harvesting infrastructure should be concentrated.

2. Materials and Methods

2.1. Study area and field-based watershed context

The Deli watershed lies in Baghmalek County, eastern Khuzestan Province, southwestern Iran, on the northeastern limb of the Asmari anticline in the folded Zagros. The setting is semi-arid and storm-driven, with marked interannual rainfall variability; because no quality-controlled local rainfall-intensity record was available, the 2005–2025 forcing was represented by CHIRPS rather than a station-derived EI30 climatology. The analyzed area was 105.20 km². Elevation ranged from 521.60 to 1313.40 m above sea level (mean 844.70 m), and mean terrain slope was 15.90°. The watershed is narrow and elongated from northwest to southeast before widening near the southern outlet. This geometry is relevant to erosion interpretation: runoff generated on steep lateral slopes is funneled towards a central drainage axis and then to the Rud-e Zard–Jarreh reservoir system.

To keep historical evidence distinct from contemporary model outputs, the previous technical assessments were used as process context, not as calibration data.

. Geological mapping identified Gachsaran, Mishan, Aghajari, Lahbari, Bakhtiari and Quaternary units; red and grey marl, siltstone and weakly cemented Aghajari materials were described as particularly erodible, whereas low-permeability fine-grained units favored rapid runoff. Field teams recorded sheet, rill, channel/gully, solution, mechanical and stream-bank erosion.

Pedological work included profile description and laboratory measurements of texture, structure, organic carbon, lime, pH, electrical conductivity and hydrological soil group. A spring 2008 survey mapped about 8,130.51 ha of rangeland (77.28% of the project area) and reported generally poor or very poor condition with a negative trend. Because the observations were not repeated annually, were not co-registered with the present raster cells and may not represent current management, they were used only to formulate process-plausibility checks and field hypotheses, not to claim validation.

2.2. Input data and common computational grid

Universal Transverse Mercator Zone 39N (EPSG:32639) and a common 30 m grid were adopted as the spatial analytical framework for raster multiplication. The authoritative watershed mask contained 116,884 active cells, equivalent to 105.20 km². Before calculation, coordinate reference system, pixel origin, dimensions, no data definition and valid coverage were checked for every input. Continuous CHIRPS and SoilGrids layers were bilinearly resampled only for grid alignment, whereas categorical land-cover and management layers used nearest-neighbor assignment.

Table 1. Input datasets, analytical roles and information-scale limitations.

Dataset	Native period / support	Role in analysis	Principal limitation
Copernicus DEM GLO-30	30 m	Slope, LS, D8 flow-routing topology, drainage and connectivity	Flow pathways remain sensitive to elevation error
Landsat 5–9 C2 L2	2005–2025; 30 m	Annual NDVI, NDMI and C after local harmonization	Residual inter-sensor and sub-pixel differences
CHIRPS Daily v2.0	2005–2025; 0.05°	Monthly rainfall, MFI and annual R proxy	No EI30; 0.05° climatic support; possible extreme-event bias
SoilGrids 2.0	~250 m	Texture, organic carbon and K sensitivity	~250 m support; 30 m alignment adds no soil information
ESA WorldCover	2020–2021; 10 m	Stable cropland and conditional P scenarios	Potential management, not observed practice
Previous technical assessments	Historical field surveys, 2008	Geology, soils, erosion and rangeland context	Not an annual or co-registered validation dataset

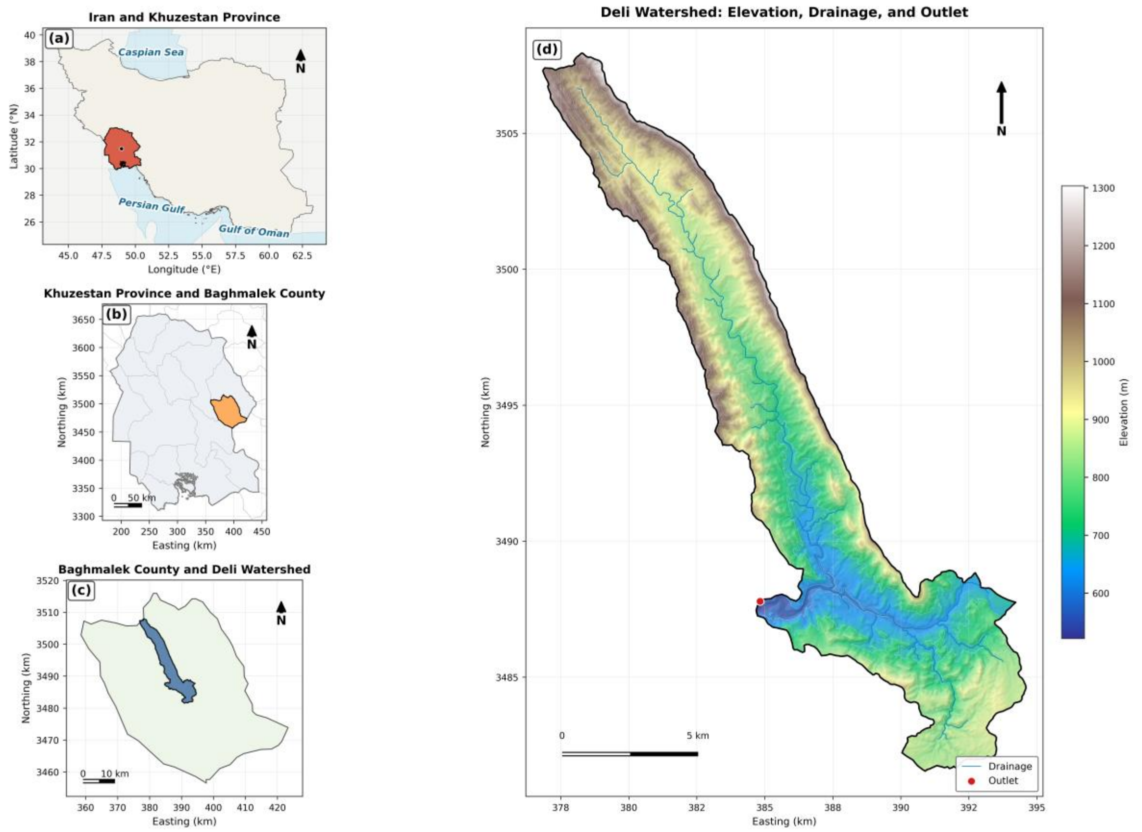

Fig. 1. Geographical setting of the Deli watershed: (a) Iran (b) Khuzestan Province (c) Baghmalek County and (d) elevation, drainage network and outlet of the Deli watershed. Source: research outputs.

Bilinear resampling can smooth contrasts across native 0.05° CHIRPS pixels; such gradients were not interpreted as independent 30 m rainfall information. The 30 m grid was selected because it matches the Landsat and DEM inputs, preserves hillslope convergence better than a 90 m grid and avoids the false precision of a 10 m grid unsupported by the 21-year Landsat series or the DEM. It is a compatibility grid, not a claim that CHIRPS or SoilGrids contains 30 m climatic or pedological detail.

2.3. Hydrological conditioning and topographic factor

The 30 m Copernicus DEM was screened for invalid cells and hydrologically conditioned before application of the D8 single-flow-direction algorithm, which assigns each cell to its steepest downslope neighbor and recursively defines contributing area. The outlet was selected by maximizing agreement between the reference watershed area and D8 contributing area. Topology was verified by requiring one valid receiver for every non-outlet cell, visiting all 116,884 active cells during topological sorting and testing for residual cycles; no cycle repair was required. A 1 km² contributing-area threshold defined the reference stream network, while 0.5 and 2 km² thresholds bracketed drainage-density sensitivity; the 1 km² value is therefore the midpoint reference rather than a unique geomorphic threshold.

The LS factor was calculated from specific contributing area and local slope following Moore and Burch (1986), with protective lower bounds to prevent division by zero. LS was held fixed because no repeat topography capable of resolving geomorphic change was available; annual surface-cover variation was represented separately by C.

2.4. Landsat processing and local cross-sensor harmonization

Landsat 5, 7, 8 and 9 Collection 2 Level 2 surface-reflectance observations were screened for 2005–2025. Quality-assurance bits were used to exclude cloud, cloud shadow, snow and saturated observations. After the collection-specific scale and offset were applied, the normalized difference vegetation index and normalized difference moisture index were calculated. In total, 1416 accepted scenes contributed to the annual composites.

Local, near-coincident Landsat 7–8 pairs were chosen instead of transferring a published global correction, because the apparent 2013 step in the preliminary series could not safely be attributed to land-surface change. Landsat 5/7 indices were transformed to an Operational Land Imager equivalent using $NDVI\_OLI = 0.027199 + 0.983485 \times NDVI\_TM/ETM+$ and $NDMI\_OLI = -0.000896 + 0.811434 \times NDMI\_TM/ETM+$. Annual median composites were then produced, along with observation counts and valid-coverage fractions. The annual cover-management factor was calculated as $C_{i,t} = \exp[-2\, NDVI_{i,t}/(1 - NDVI_{i,t})]$ and constrained to 0–1 (Eq. 2; Van der Knijff et al. 2000).

C varies annually, whereas LS is static, because the former represents surface protection and the latter represents unresolved terrain geometry. The empirical NDVI–C conversion was not field-calibrated in Deli; its structural sensitivity was therefore carried into the low/high envelope. Local sensor harmonization reduces the risk of interpreting spectral response as land-surface change but cannot remove all effects of view geometry, atmospheric correction or sub-pixel composition (Roy et al. 2016; Xiong et al. 2023).

2.5. Rainfall-erosivity proxy

Daily CHIRPS v2.0 precipitation was aggregated first to monthly and annual totals. MFI was calculated from monthly and annual precipitation (Eq. 3), and the reference rainfall-erosivity proxy used the piecewise Renard–Freimund MFI equations (Eqs. 4a–b); the alternative annual-precipitation equations (Eqs. 5a–b) defined the structural sensitivity case (Renard and Freimund 1994). P and MFI are in millimeters and the derived R proxy retains the conventional MJ mm ha^{-1} h^{-1} yr^{-1} scaling, but it is not a locally measured EI30 factor. Annual CHIRPS surfaces were bilinearly aligned to the 30 m grid after temporal aggregation.

This interpolation smooths boundaries between 0.05° pixels but does not create sub-pixel climatic information. CHIRPS was not independently validated against a quality-controlled local gauge record, and its potential attenuation of short convective extremes can bias R downward and alter the relative height of annual peaks. Consequently, R is termed a rainfall-erosivity proxy throughout and its spatial texture is interpreted only at native-product support.

2.6. Soil erodibility and support-practice scenarios

SoilGrids sand, silt, clay and organic-carbon layers for 0–5, 5–15 and 15–30 cm were combined as thickness-weighted 0–30 cm means using weights 5/30, 10/30 and 15/30. K was then calculated with the Williams–Renard EPIC pedotransfer equation and converted to SI units by 0.1317 (Eq. 6; Williams et al. 1983; Benavidez et al. 2018). The mean reference K was 0.0363 Mg h MJ^{-1} mm^{-1}; lower and upper alternatives represented depth and pedotransfer sensitivity. Because SoilGrids has an effective support of approximately 250 m, its 30 m representation was used only for numerical alignment and no sub-250 m soil pattern was interpreted. In the absence of a georeferenced inventory of observed practices and construction dates, baseline P = 1 was retained as a conservative no-practice reference; it can overestimate potential erosion where effective terraces or other practices already exist and is not a map of actual management.

Moderate and strong scenarios were restricted to cropland mapped consistently in the 2020 and 2021 ESA WorldCover products (Zanaga et al. 2022) and to slopes ≤30°. Across eligible cells, the slope-dependent P assignments represented 10–45% reductions in the moderate scenario and 55–72.5% reductions in the strong scenario. The 30° ceiling is an explicit scenario-domain rule, not an engineering suitability threshold; a 20° ceiling would test a narrower treatment domain and requires locally observed practice data. The resulting stable, slope-eligible area was 4.85 km^2. Both scenarios are conditional experiments rather than observations of contour farming, terracing or check-dam performance. Because structure coordinates, installation dates and performance records were unavailable, no temporal change was attributed to existing watershed works.

2.7. Dynamic erosion, connectivity and uncertainty analysis

For every active cell i, year t and management scenario s, the aligned R, K, LS, C and P layers were multiplied cell by cell according to Eq. 7. Watershed summaries are equal-area statistics across the valid 30 m cells; no cross-resolution averaging was performed after multiplication. The numerical product was retained for within-study comparison and ranking but was not assigned mass-per-area units because no plot, suspended-sediment or reservoir-survey observations were available for calibration. Low and high structural cases combined alternative R, K, C and P assumptions, and their difference defines a sensitivity envelope rather than a confidence interval or probability distribution.

Structural sediment connectivity was calculated as the base-10 logarithm of the ratio of upslope source potential to downslope impedance along the D8 route to the 1 km^2 reference stream network (Eqs. 8–10; Borselli et al. 2008; Cavalli et al. 2013; Crema and Cavalli 2018). The upslope term combines mean weight, mean slope and square root of contributing area; the downslope term accumulates cell length divided by weight and slope. Unit weight was used for the static topographic implementation, while annual C represented surface resistance in the dynamic implementation. The relative sediment-delivery proxy is the cell-wise product of long-term source potential and normalized structural connectivity; high values therefore require both a strong source and a comparatively efficient structural pathway. It is an empirical rank, not a measured sediment-delivery ratio or event-scale flux.

Within each year, the watershed-specific 90th percentile was selected a priori as a transparent upper-decile screen, retaining the same 10% area despite strong interannual amplitude differences. An 85th or 95th percentile would retain a broader or narrower fraction, respectively; none is a confidence limit or field-calibrated erosion threshold (Panagos et al. 2020; La Licata et al. 2025). Persistence is the percentage of 21 years in which a cell remained in that upper decile; the ≥50% and ≥75% classes correspond to at least 11 and 16 years and are descriptive recurrence thresholds.

Percentile ranks of erosion potential, relative delivery, persistence and structural uncertainty were combined into an integrated priority index. Five equal-area classes were used to provide comparable 20% screening inventories and avoid implying unsupported natural breakpoints.

The index organizes reconnaissance and monitoring; it does not replace engineering design, land-tenure assessment or site-specific feasibility analysis.

Variables and units: NIR, Red, $SWIR_1$, NDVI, NDMI, C, P, LS, W and S are dimensionless; $P_{m,t}$ and P_t are precipitation (mm); MFI is in mm; R is a rainfall-erosivity proxy (MJ mm ha^{-1} h^{-1} yr^{-1}); Sa, Si and Cl are sand, silt and clay (%), OC is organic carbon (%), SN = 1 − Sa/100, and K_SI is Mg h MJ^{-1} mm^{-1}. Aup is contributing area (m^2), d is flow-path length (m), IC and its normalized form are dimensionless, Urel is %, and the uncalibrated A and Drel products are reported only in relative index units.

Table 2. Principal equations and computational components.

Component	Numbered expression / implementation
Spectral indices	$NDVI = (NIR - Red)/(NIR + Red)$; $NDMI = (NIR - SWIR_1)/(NIR + SWIR_1)$ (1a,b)
Cover-management factor	$C_{i,t} = \exp[-2\ NDVI_{i,t}/(1 - NDVI_{i,t})]$, constrained to 0–1 (2)
Modified Fournier index	$MFI_t = \Sigma_{m=1}^{12}(P_{m,t}^2/P_t)$ (3)
MFI-based R proxy	$R_t = 0.07397\ MFI_t^{1.847}$ for $MFI < 55$; $R_t = 95.77 - 6.081MFI_t + 0.4770MFI_t^2$ otherwise (4a, b)
Annual-precipitation R proxy	$R_t^P = 0.04830\ P_t^{1.610}$ for $P < 850$; $R_t^P = 587.8 - 1.219P_t + 0.004105P_t^2$ otherwise (5a,b)
Soil erodibility	$K\_US = [0.2 + 0.3\exp(-0.0256Sa(1 - Si/100))](Si/(Cl + Si))^{0.3}[1 - 0.25OC/(OC + \exp(3.72 - 2.95OC))][1 - 0.7SN/(SN + \exp(-5.51 + 22.9SN))]$; $K\_SI = 0.1317K\_US$ (6)
Annual erosion index	$A_{i,t,s} = R_tK_iLS_iC_{i,t}P_{i,s}$ (7)
Connectivity index	$IC_i = \log_{10}(Dup_{,i}/Ddn_{,i})$ (8)
Upslope component	$Dup_{,i} = \bar{W}_i\bar{S}_i\sqrt{Aup_{,i}}$ (9)
Downslope component	$Ddn_{,i} = \Sigma_{j\rightarrow stream}[d_j/(W_jS_j)]$ (10)
Relative uncertainty	$Urel = 100(Ahigh - Alow)/Aref$ (11)
Relative delivery proxy	$Drel_{,i} = Along\text{-}term_{,i} \times ICnorm_{,i}$ (12)

2.8. Statistical analysis and quality assurance

Pixel-wise temporal change was summarized by Sen's slope, the median of all pairwise annual slopes. Monotonic watershed-scale association with time was tested using two-sided Spearman rank correlation at $\alpha = 0.05$ (Sen 1968). Spearman rather than Pearson correlation was selected because $n = 21$, annual responses include large peaks and no linear-normal residual model was assumed. Correlations of annual watershed means of R and C with A were retained only as endogenous diagnostics of model behavior because R and C are mathematical inputs to A; they are not independent evidence of causality. The earlier standardized regression and its coefficients were removed, so residual-based inference is not claimed. Equal-area watershed means can suppress local contrasts, and raster-cell dependence precludes treating pixels as independent replicates for spatial significance testing.

Quality assurance checked annual completeness, finite values, factor ranges, raster alignment, scenario ordering and full priority-class coverage. D8 verification required a single receiver or outlet per cell, complete topological traversal and zero residual cycles; the recomputed connectivity surface was also compared with the independent processing reference. These checks establish computational coherence, not field validation.

3. Results and Discussion

3.1. Computational coherence and annual dynamics

All 21 annual composites passed coverage and finite-value checks. The D8 flow-routing topology included every active watershed cell, required no cycle repair and identified 1,985 stream cells at the 1 km^2 threshold. Recomputed topographic connectivity agreed closely with the independent processing reference ($r = 0.999$; RMSE = 0.043). This verifies routing and index implementation only; it does not validate actual sediment transfer.

The long-term baseline potential soil-loss index had a watershed mean of 582.11, a median of 438.38 and a 95th percentile of 1484.17. These values cannot be compared with physical severity thresholds in Mg ha^{-1} yr^{-1}; 582.11 denotes relative position and contrast within this modelling system only. Annual watershed means varied by more than a factor of 7.5: 2018 produced the highest response (1040.20), whereas 2010 produced the lowest (138.33).

The 2018 maximum coincided with the highest CHIRPS-derived erosivity proxy, while K and LS were fixed and C varied over a much narrower range. This is an internal model attribution, not independent evidence of measured erosion intensity or climate change.

The watershed-scale Sen's slope was +3.72 relative index units yr^{-1}, but association with time was negligible and non-significant (Spearman $\rho = 0.049$, $p = 0.832$). The late-period mean was 11.24% greater than the early-period mean, but a few high-erosivity years strongly influenced that contrast. Accordingly, the record does not demonstrate a monotonic climate-change signal. Without local gauges or EI30 observations, abrupt peaks cannot be separated conclusively from natural climatic variability and CHIRPS error; they are treated as proxy-driven model variability.

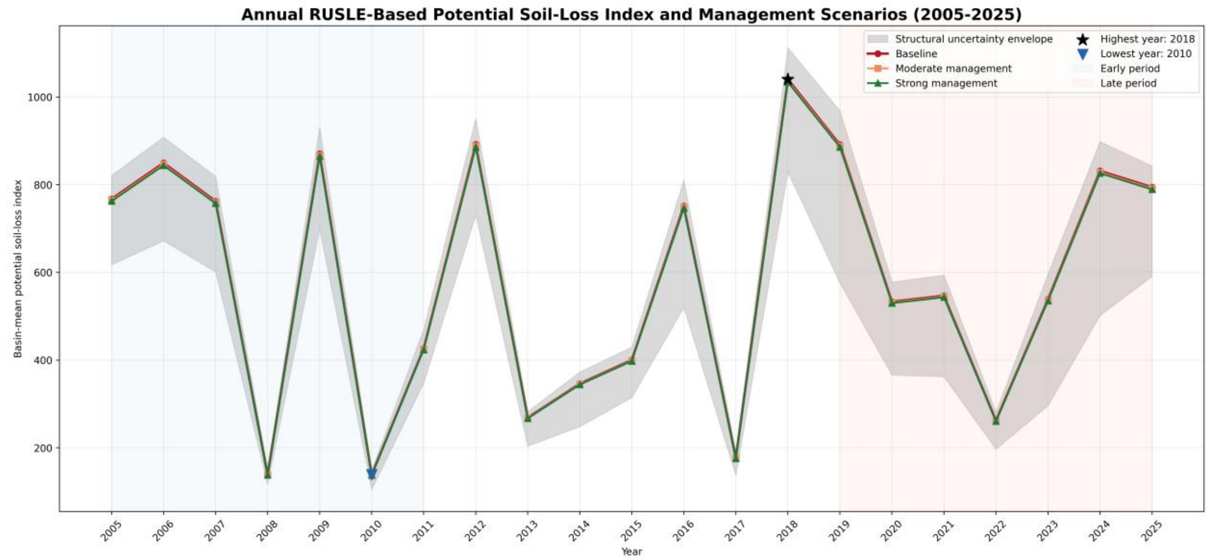

Fig. 2. Annual RUSLE-based potential soil-loss index under baseline, moderate and strong management scenarios, 2005–2025. The grey band shows the structural sensitivity envelope; symbols identify the highest and lowest years.

3.2. Temporal controls on the annual response

The rainfall-erosivity proxy varied over a much wider annual range than the watershed-mean C factor. Erosivity was low in 2008, 2010 and 2017 and high in 2018, 2019, 2024 and 2025. The harmonized C factor declined from values near 0.78 in several early years to 0.68 in 2023, before rising again by 2025. Because a larger C denotes less surface protection, that partial decline would tend to moderate erosion; it cannot explain the largest annual peaks.

The annual baseline response was strongly associated with the rainfall-erosivity proxy (Spearman $\rho = 0.98$, $p < 0.001$), whereas its association with the watershed-mean C factor was weak and non-significant ($\rho = -0.07$, $p = 0.758$). Because both R and C are multiplicative inputs to A, these correlations describe internal model sensitivity and do not estimate physical weights or causal effects. No regression coefficients are reported.

The weak watershed-mean C correlation does not quantify a local vegetation effect: equal-area averaging suppresses spatial contrasts and the annual C range was much narrower than the R range.

The 2008 reports may describe historical process settings but cannot establish current management or validate local C responses. Interpretation is therefore limited to the observed model behavior: R explains most year-to-year amplitude within the multiplicative index, while the spatial pattern reflects the combined fixed and dynamic input layers and remains a hypothesis for field testing.

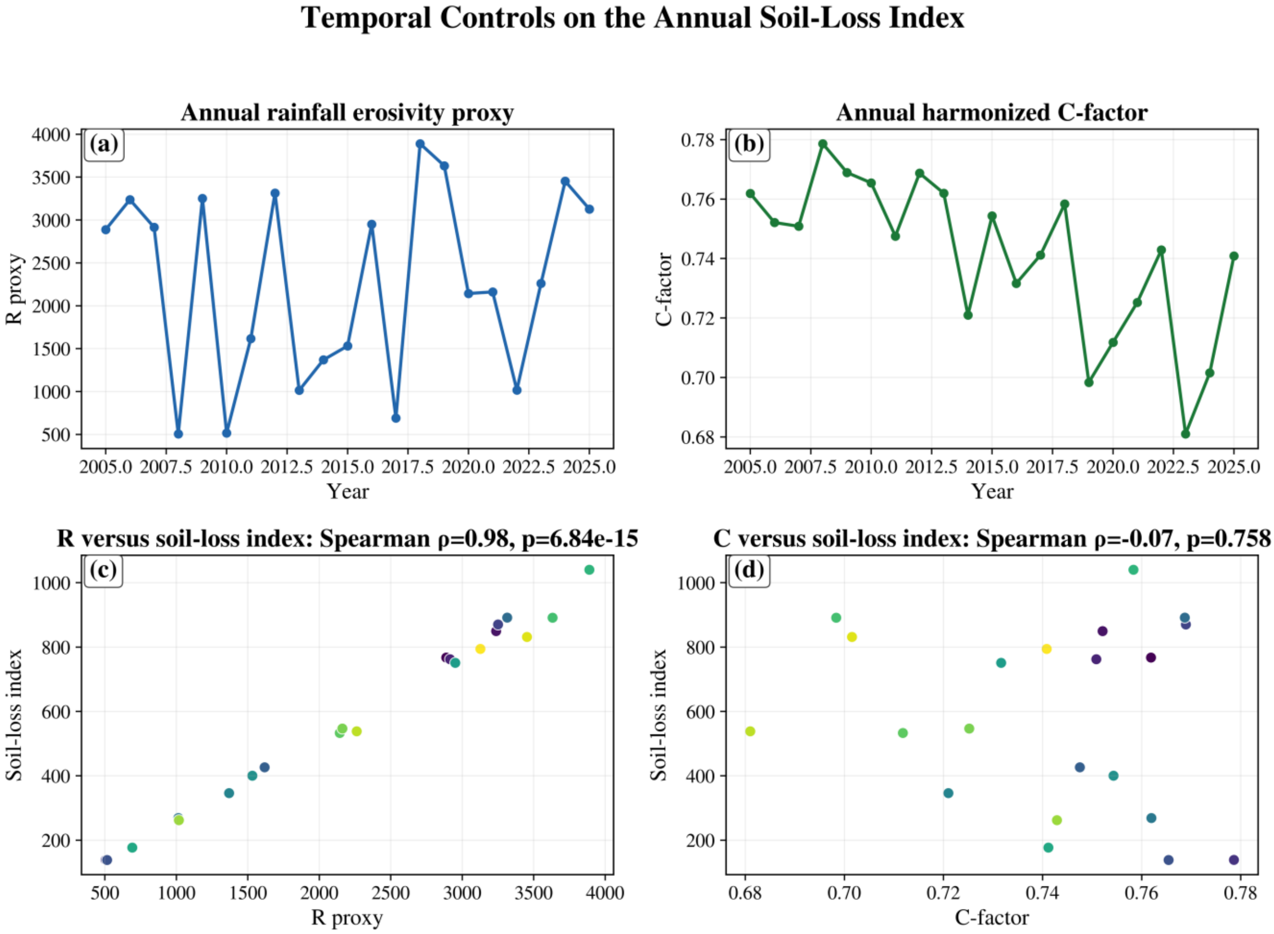

Fig. 3. Temporal controls on the annual response: rainfall-erosivity proxy, harmonized C factor and their rank relationships with the watershed-mean potential soil-loss index. Correlations are endogenous model diagnostics; all index values are relative.

3.3. Spatial pattern, connectivity and persistent hotspots

Spatial cross-comparison showed partial rather than complete overlap between high source potential and high structural connectivity. The strongest co-occurrence followed steep, convergent and channel-adjacent bands, whereas some high-erosion patches on divides or upper slopes had longer, gentler or more resistant pathways and therefore lower delivery-proxy ranks. Thus, high erosion potential alone does not define a sediment-delivery hotspot; the relative delivery proxy screens for the intersection of source magnitude and structural connection to the stream network.

Pixel-wise Sen slopes were positive in parts of the southern watershed and along channel-adjacent terrain, while several northern areas were stable or negative. Because slope, soil, cover and flow convergence covary spatially, the north–south contrast cannot be attributed uniquely to land-use change, soil or relief without independent spatial attribution data.

Cells classified as hotspots in at least 11 of 21 years (≥50% persistence) occupied 10.42 km², or about 9.9% of the watershed; 9.17 km² remained hotspots in at least 16 years (≥75%). The small area difference indicates stable relative ranking across contrasting forcing years. These are recurrence classes based on annual upper-decile membership, not confidence intervals or repeated exceedance of a universal erosion rate.

The 2008 technical assessments describe erodible marl–siltstone, rilling, gullying, bank erosion and fine-material movement towards Jarreh Reservoir, but their age and lack of co-registered maps prevent quantitative validation or inference about present conditions. Accordingly, spatial correspondence is used only to formulate locations and processes for renewed field inspection; it is not evidence of model accuracy.

Connectivity changes the management meaning of an erosion map: cells with similar source potential can have different pathway impedances and downstream relevance. This source–pathway–target logic is consistent with agricultural and mountain studies (Batista et al. 2022; La Licata et al. 2025) and with channel-centred structural pathways reported for the Abolabbas watershed in Khuzestan (Zoratipour and Heidary 2022). However, absolute IC values are not directly transferable among catchments because DEM resolution, target-network threshold, weighting and normalization differ. In the folded Zagros, structurally guided drainage and narrow convergent slopes make IC useful for relative screening, while event discharge, temporary storage, barriers, gully enlargement and in-channel remobilization remain unmodelled.

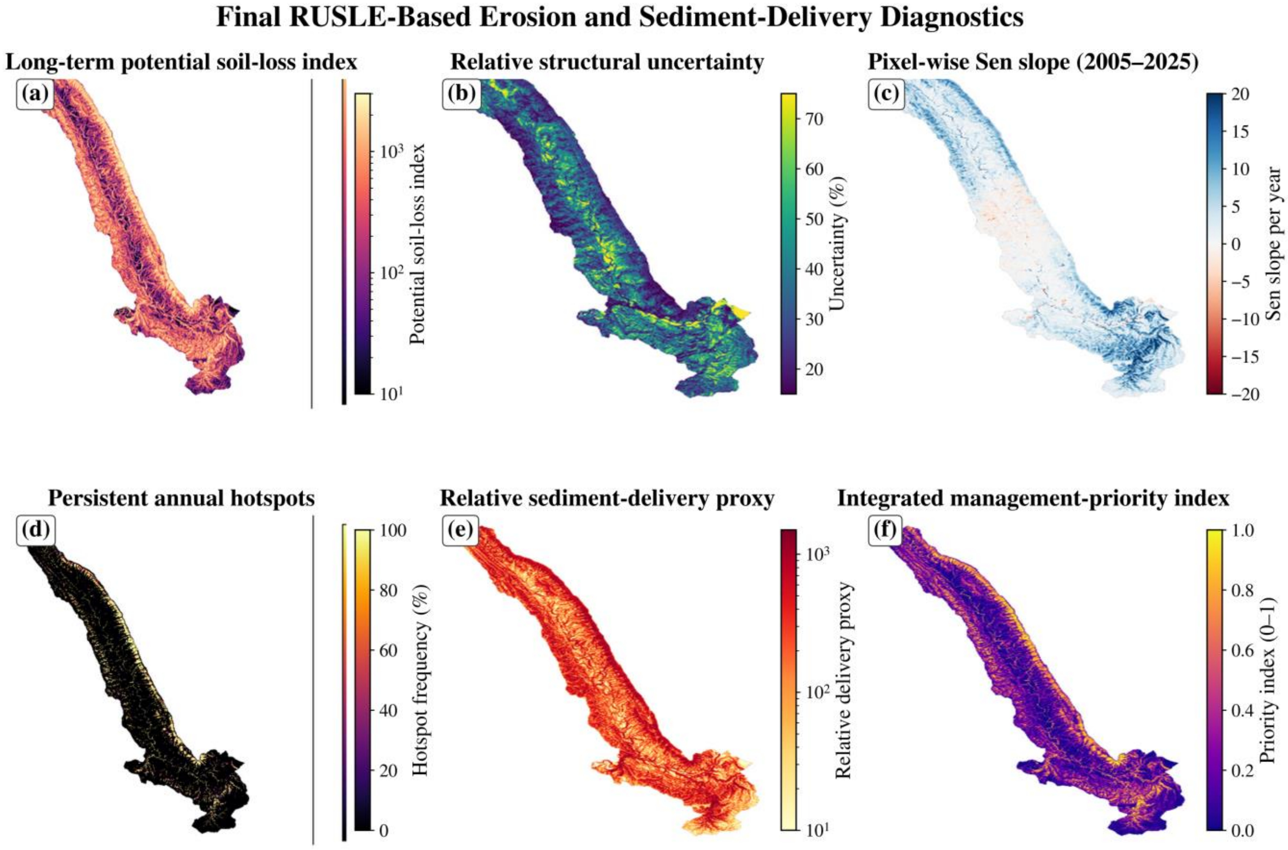

Fig. 4. Spatial diagnostics: (a) long-term potential soil-loss index (relative index units), (b) structural uncertainty (%), (c) Sen slope (relative index units yr^{-1}), (d) hotspot persistence (%), (e) relative sediment-delivery proxy (relative index units) and (f) integrated priority index (0–1). All panels use the same watershed extent.

3.4. Structural uncertainty

The mean absolute sensitivity range was 196.19 relative index units and mean relative structural uncertainty was 37.40%. The 20–40% class covered 55.08% of the watershed and the 40–60% class covered 28.31%. Relative uncertainty did not rise monotonically with erosion class: some high-response cells retained stable ranks across assumptions, whereas lower-reference cells could show large percentages because a similar absolute range was divided by a smaller denominator. Hence, uncertainty percentages and erosion magnitude must be consulted together rather than interpreted as a single error rate.

The sensitivity envelope represents alternative defensible R, K, C and P choices; it is neither a confidence interval nor a probability distribution. High-potential, well-connected cells with moderate uncertainty are candidates for early reconnaissance, whereas high-priority cells with high uncertainty require measurement before costly intervention. No economic benefit is inferred from the map alone.

Intrinsic input and model uncertainties remain important. Landsat annual medians reduce cloud contamination but retain atmospheric, sensor, view-geometry and mixed-pixel effects; CHIRPS may smooth or underestimate short convective extremes and has 0.05° rather than 30 m climatic support. SoilGrids represents approximately 250 m support, so resampling can visually sharpen boundaries without adding soil information and may suppress local pedological variability. The empirical IC is sensitive to DEM error, D8 routing, stream-threshold choice and surface weighting, and it omits discharge, temporary storage and barrier failure. These limitations affect absolute interpretation more strongly than relative ranking and are not fully represented by the structural envelope.

3.5. Conservation scenarios and scale dependence

The long-term mean potential soil-loss index declined from 582.11 relative index units under baseline P = 1 to 580.15 under moderate management and 578.42 under strong management. These changes equal watershed-wide reductions of 0.34% and 0.63%. Within the 4.85 km² eligible cropland, the mean reductions were 36.87% and 68.38%. The study does not include implementation costs or benefits, so these percentages cannot establish economic feasibility; they only compare conditional model responses. Scenario ordering (strong ≤ moderate ≤ baseline) held for every valid cell.

The contrast between local and whole-watershed effectiveness is a scale effect, not evidence that conservation is ineffective. Eligible cropland represented about 4.6% of the watershed, and the targeted parcels differed in baseline erosion and structural connectivity. A large proportional reduction over a small or weakly connected area scarcely changes the watershed mean, whereas treatment at a connected bottleneck may have greater downstream relevance (Pérez-Cutillas et al. 2026; Alsaihani and Alharbi 2024).

Cropland-only treatment does not represent all processes described historically in Deli, including degraded rangeland, exposed marl, concentrated flow and bank instability. A field programme may therefore examine grazing regulation, recovery of perennial cover, contour-oriented roughness, concentrated-flow stabilization, small retention structures and bank protection. The model does not select engineering designs; each candidate site requires field confirmation of process, tenure, foundation conditions, storage, safe overflow and downstream risk.

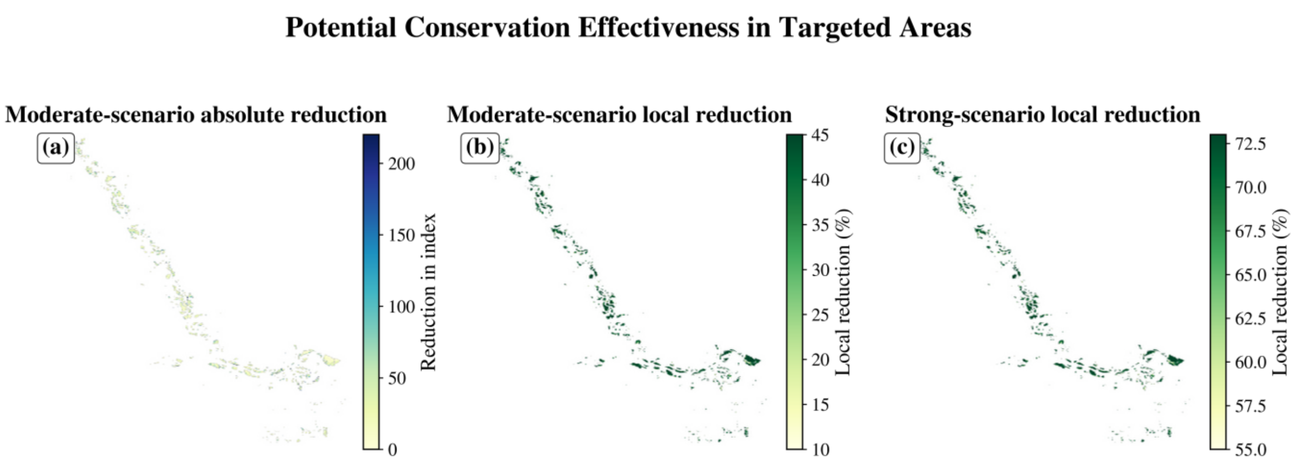

Fig. 5. Potential conservation effectiveness in 4.85 km² of eligible stable cropland: moderate-scenario absolute reduction (relative index units) and local reductions (%) under moderate and strong scenarios.

3.6. Integrated priorities for water-harvesting and sediment-control planning

Using the pre-defined equal-area quintiles described in Section 2.7, the very-high-priority class occupied 21.04 km² (approximately 20% of the watershed), with mean erosion potential of 1418.22 and mean relative delivery proxy of 870.46. These means were about 16 and 25 times those of the very-low class, and nearly half of all annual hotspot occurrences fell within the very-high class. This joint contrast confirms that the top class concentrates source intensity, persistence and structural connection rather than cells extreme in only one layer.

For water-harvesting planning, the priority layer is a first-tier screening tool to rank field visits, monitoring and possible sediment pre-treatment. It must be combined with measured runoff and sediment, storage geometry, geotechnical conditions, land ownership and downstream safety before design. A high-priority source upstream of a proposed structure signals potential sediment burden; it does not by itself identify a safe construction site.

The history of watershed structures could not be incorporated because their exact locations, construction dates and performance records were unavailable. No claim was therefore made that the 2013 sensor-era discontinuity or any later change resulted from check dams or other works. A useful future inventory should record structure type, crest and spillway dimensions, sediment depth, storage loss, failure status, maintenance history and contributing area. Combining such an inventory with persistent hotspots and connected pathways would permit a defensible before–after or control–impact evaluation.

Table 3. Principal quantitative results and management-scenario effects.

Indicator	Value	Units	Interpretation
Long-term baseline means	582.11	relative index units	Relative potential soil-loss index
Long-term median / 95th percentile	438.38 / 1484.17	relative index units	Spatial distribution
Highest / lowest annual mean	2018: 1040.20 / 2010: 138.33	relative index units	Annual extremes
Watershed Sen slope	+3.72	relative index units yr^{-1}	Non-significant; time $\rho = 0.049$, $p = 0.832$
R proxy vs annual response	$\rho = 0.98$; $p < 0.001$	dimensionless (ρ and p)	Strong endogenous diagnostic association
C factor vs annual response	$\rho = -0.07$; $p = 0.758$	dimensionless (ρ and p)	Weak, non-significant watershed-mean association
Hotspot persistence ≥50% / ≥75%	10.42 / 9.17 km^2	km^2	Persistent upper-decile source areas
Mean relative structural uncertainty	37.40%	%	Sensitivity envelope, not a confidence interval
Moderate / strong local reduction	36.87% / 68.38%	%	Within 4.85 km^2 of targeted stable cropland
Moderate / strong watershed reduction	0.34% / 0.63%	%	Effect after averaging across the watershed
Very-high management-priority area	21.04 km^2	km^2	Approximately 20% of the watershed

3.7. Limitations and transferability

The principal limitation is the absence of independent observations of plot erosion, suspended sediment, bedload or reservoir deposition; all RUSLE and delivery products therefore remain relative screening indices. The workflow does not simulate gully enlargement, landsliding, stream-bank erosion, explicit deposition or hydrological/functional connectivity. Conditional P scenarios are not observed practice, and the 21-year record limits trend power. These constraints prevent physical validation, probabilistic uncertainty analysis and causal attribution; numerical detail must not be interpreted as physical accuracy.

Fitted sensor coefficients, NDVI–C conversion, K pedotransfer estimates, drainage threshold, P scenarios and priority weights are context dependent and should not be transferred unchanged. What is transferable is the reproducible screening sequence: harmonies sensors, preserve native-scale warnings, distinguish source potential from structural transfer potential, test persistence, compare local and watershed scales, and carry sensitivity into prioritization. Moving from screening to calibrated decision support requires event-scale rainfall and runoff monitoring, suspended-sediment and bedload sampling, reservoir or structure sediment surveys, targeted soil/cover measurements and a georeferenced inventory of existing works.

4. Conclusion

By combining locally harmonized Landsat observations, CHIRPS rainfall, SoilGrids, a hydrologically conditioned DEM, annual RUSLE calculations, structural connectivity and conditional management scenarios, twenty-one years of relative erosion behavior were modelled in the Deli watershed. The annual record was highly variable but showed no significant monotonic watershed trend. The first part of the working hypothesis was supported within the model: the R proxy governed most interannual amplitude. The second part was also supported as a structural pattern—persistent hotspots clustered on steep, convergent and connected terrain—but remains unvalidated as actual sediment transfer.

Persistent upper-decile hotspots occupied 10.42 km² in at least 11 years and 9.17 km² in at least 16 years. The very-high integrated class occupied 21.04 km² and jointly concentrated high source and delivery-proxy ranks. Historical reports identify processes for renewed reconnaissance but do not validate the maps. Accordingly, the products should receive screening-level weight: they can rank survey and monitoring effort, but high-uncertainty sites require independent measurement and no structure should be located or designed from the maps alone.

Support-practice scenarios produced large local reductions in eligible cropland but small changes in the watershed mean because only about 4.6% of the area was treated. Treatment extent and structural position therefore matter as much as nominal intensity. Operationally, managers may use the very-high class to sequence field inspection, measure sediment pathways and assess whether pre-treatment or distributed retention is warranted before any water-harvesting design.

Mean relative structural uncertainty of 37.40% and the absence of sediment observations require conservative use. The products are comparative indices, not Mg ha^{-1} yr^{-1} or measured sediment yield. Priority research is therefore to (i) establish event-scale rainfall–runoff and suspended-sediment stations, (ii) survey bedload and reservoir/structure deposition, (iii) sample soil erodibility and seasonal cover in representative high-priority classes, and (iv) inventory existing structures with dates and performance. These data would permit calibration, probabilistic uncertainty analysis and before–after or control–impact evaluation.

5. Acknowledgements

The authors acknowledge the field specialists and technical teams who prepared the previous geology, hydrology, pedology, erosion and rangeland technical assessments for the Deli watershed. Their observations provided historical process context for the present geospatial analysis.

6. Conflict of interest

No potential conflict of interest was reported by the authors.

7. References

Alsaihani, M., & Alharbi, R. (2024). Mapping of soil erosion vulnerability in Wadi Bin Abdullah using remote sensing and GIS techniques. *Water, 16*(18), 2663. https://doi.org/10.3390/w16182663

Barbadori, F., Confuorto, P., Chouksey, B., Moretti, S., & Raspini, F. (2024). Multi-temporal assessment of soil erosion after a wildfire in Tuscany using Google Earth Engine. *Land, 13*(11), 1950. https://doi.org/10.3390/land13111950

Batista, P. V. G., Fiener, P., Scheper, S., & Alewell, C. (2022). A conceptual-model-based sediment connectivity assessment for patchy agricultural catchments. *Hydrology and Earth System Sciences, 26*, 3753–3770. https://doi.org/10.5194/hess-26-3753-2022

Benavidez, R., Jackson, B., Maxwell, D., & Norton, K. (2018). A review of the (Revised) Universal Soil Loss Equation. *Hydrology and Earth System Sciences, 22*, 6059–6086. https://doi.org/10.5194/hess-22-6059-2018

Borrelli, P., Alewell, C., Alvarez, P., Anache, J. A. A., Baartman, J., Ballabio, C., Bezak, N., Biddoccu, M., Cerdà, A., Chalise, D., Chen, S., Chen, W., De Girolamo, A. M., Gessesse, G. D., Deumlich, D., Diodato, N., Efthimiou, N., Erpul, G., Fiener, P., … Panagos, P. (2021). Soil erosion modelling: A global review and statistical analysis. *Science of the Total Environment, 780*, 146494. https://doi.org/10.1016/j.scitotenv.2021.146494

Borrelli, P., Robinson, D. A., Panagos, P., Lugato, E., Yang, J. E., Alewell, C., Wuepper, D., Montanarella, L., & Ballabio, C. (2020). Land use and climate change impacts on global soil erosion by water (2015–2070). *Proceedings of the National Academy of Sciences, 117*(36), 21994–22001. https://doi.org/10.1073/pnas.2001403117

Borselli, L., Cassi, P., & Torri, D. (2008). Prolegomena to sediment and flow connectivity in the landscape: A GIS and field numerical assessment. *Catena, 75*(3), 268–277. https://doi.org/10.1016/j.catena.2008.07.006

Cavalli, M., Trevisani, S., Comiti, F., & Marchi, L. (2013). Geomorphometric assessment of spatial sediment connectivity in small Alpine catchments. *Geomorphology, 188*, 31–41. https://doi.org/10.1016/j.geomorph.2012.05.007

Crema, S., & Cavalli, M. (2018). SedInConnect: A stand-alone, free and open source tool for the assessment of sediment connectivity.

Computers & Geosciences, 111, 39–45. https://doi.org/10.1016/j.cageo.2017.10.009

Deli Watershed Detailed Studies Project. (2008a). Geology, hydrology, meteorology and physiography reports for the Deli watershed [Unpublished executive project reports in Persian]. Khuzestan Province, Iran.

Deli Watershed Detailed Studies Project. (2008b). Pedology, erosion, rangeland and forest reports for the Deli watershed [Unpublished executive project reports in Persian]. Khuzestan Province, Iran.

Funk, C., Peterson, P., Landsfeld, M., Pedreros, D., Verdin, J., Shukla, S., Husak, G., Rowland, J., Harrison, L., Hoell, A., & Michaelsen, J. (2015). The Climate Hazards Infrared Precipitation with Stations—A new environmental record for monitoring extremes. *Scientific Data, 2*, 150066. https://doi.org/10.1038/sdata.2015.66

Gorelick, N., Hancher, M., Dixon, M., Ilyushchenko, S., Thau, D., & Moore, R. (2017). Google Earth Engine: Planetary-scale geospatial analysis for everyone. *Remote Sensing of Environment, 202*, 18–27. https://doi.org/10.1016/j.rse.2017.06.031

Heckmann, T., Cavalli, M., Cerdan, O., Foerster, S., Javaux, M., Lode, E., Smetanová, A., Vericat, D., & Brardinoni, F. (2018). Indices of sediment connectivity: Opportunities, challenges and limitations. *Earth-Science Reviews, 187*, 77–108. https://doi.org/10.1016/j.earscirev.2018.08.004

La Licata, M., Bosino, A., Sadeghi, S. H., De Amicis, M., Mandarino, A., Terret, A., & Maerker, M. (2025). HOTSED: A new integrated model for assessing potential hotspots of sediment sources and related sediment dynamics at watershed scale. *International Soil and Water Conservation Research, 13*(1), 80–101. https://doi.org/10.1016/j.iswcr.2024.06.002

Moore, I. D., & Burch, G. J. (1986). Physical basis of the length-slope factor in the Universal Soil Loss Equation. *Soil Science Society of America Journal, 50*(5), 1294–1298. https://doi.org/10.2136/sssaj1986.03615995005000050042x

Najafi, S., Dragovich, D., Heckmann, T., & Sadeghi, S. H. (2021). Sediment connectivity concepts and approaches. *Catena, 196*, 104880. https://doi.org/10.1016/j.catena.2020.104880

Panagos, P., Ballabio, C., Poesen, J., Lugato, E., Scarpa, S., Montanarella, L., & Borrelli, P. (2020). A soil erosion indicator for supporting agricultural, environmental and climate policies in the European Union. *Remote Sensing, 12*(9), 1365. https://doi.org/10.3390/rs12091365

Pérez-Cutillas, P., Benabdelouahab, S., & Salhi, A. (2026). Mitigating erosion and enhancing sediment retention through sustainable land management scenarios. *Earth Systems and Environment, 10*, 1147–1166. https://doi.org/10.1007/s41748-025-00660-9

Poggio, L., de Sousa, L. M., Batjes, N. H., Heuvelink, G. B. M., Kempen, B., Ribeiro, E., & Rossiter, D. (2021). SoilGrids 2.0: Producing soil information for the globe with quantified spatial uncertainty. *SOIL, 7*, 217–240. https://doi.org/10.5194/soil-7-217-2021

Renard, K. G., & Freimund, J. R. (1994). Using monthly precipitation data to estimate the R-factor in the revised USLE. *Journal of Hydrology, 157*, 287–306. https://doi.org/10.1016/0022-1694(94)90110-4

Renard, K. G., Foster, G. R., Weesies, G. A., McCool, D. K., & Yoder, D. C. (1997). Predicting soil erosion by water: A guide to conservation planning with the Revised Universal Soil Loss Equation (RUSLE). USDA Agriculture Handbook No. 703. https://www.tucson.ars.ag.gov/unit/publications/PDFfiles/717.pdf

Roy, D. P., Kovalskyy, V., Zhang, H. K., Vermote, E. F., Yan, L., Kumar, S. S., & Egorov, A. (2016). Characterisation of Landsat-7 to Landsat-8 reflective wavelength and normalised difference vegetation index continuity. *Remote Sensing of Environment, 185*, 57–70. https://doi.org/10.1016/j.rse.2015.12.024

Sen, P. K. (1968). Estimates of the regression coefficient based on Kendall's tau. *Journal of the American Statistical Association, 63*(324), 1379–1389. https://doi.org/10.1080/01621459.1968.10480934

Shi, C., Liang, Y., Qin, W., Ding, L., Cao, W., Zhang, M., & Zhang, Q. (2025). Review of sediment connectivity: Conceptual connotations, characterization indicators, and their relationships with soil erosion and sediment yield. *Earth-Science Reviews, 264*, 105091. https://doi.org/10.1016/j.earscirev.2025.105091

Van der Knijff, J. M., Jones, R. J. A., & Montanarella, L. (2000). *Soil erosion risk assessment in Europe*. EUR 19044 EN. Office for Official Publications of the European Communities, Luxembourg, 34 pp.

Williams, J. R., Renard, K. G., & Dyke, P. T. (1983). EPIC: A new method for assessing erosion's effect on soil productivity. *Journal of Soil and Water Conservation, 38*(5), 381–383. https://doi.org/10.1080/00224561.1983.12436327

Xiong, M., Leng, G., & Tang, Q. (2023). Global analysis of the cover-management factor for soil erosion modelling. *Remote Sensing, 15*(11), 2868. https://doi.org/10.3390/rs15112868

Zanaga, D., Van De Kerchove, R., Daems, D., De Keersmaecker, W., Brockmann, C., Kirches, G., Wevers, J., Cartus, O., Santoro, M., Fritz, S., Lesiv, M., Herold, M., Tsendbazar, N.-E., Xu, P., Ramoino, F., & Arino, O. (2022). ESA WorldCover 10 m 2021 v200. Zenodo. https://doi.org/10.5281/zenodo.7254221

Zoratipour, A., & Heidary, K. (2022). Cell-scale sediment variation using the structural connectivity index: Abolabbas watershed, Khuzestan Province. *Iranian Journal of Soil and Water Research, 53*(6), 1213–1226. https://doi.org/10.22059/ijswr.2022.340158.669224